Subjective Surfaces: A Method for Completing Missing Boundaries

Alessandro Sarti, Ravi Malladi, and James A. Sethian

Lawrence Berkeley National Laboratory
and
Department of Mathematics
University of California
Berkeley, CA 94720

April 18, 2000

Abstract

We present a model and algorithm for segmentation of images with missing boundaries. In many situations, the human visual system fills in missing gaps in edges and boundaries, building and completing information that is not present. This presents a considerable challenge in computer vision, since most algorithms attempt to exploit existing data. Completion models, which postulate how to construct missing data, are popular, but are often trained and specific to particular images. In this paper, we take the following perspective: we consider a reference point within an image as given, and then develop an algorithm which tries to build missing information on the basis of the given point of view and the available information as boundary data to the algorithm. We test the algorithm on some standard images, including the classical triangle of Kanizsa and low signal/noise ratio medical images.

1 Introduction

Consider the images in Figure 1. It is apparent in all three images that internal boundaries exist. In the image on the left, a solid triangle in the center of the figure appears to have well-defined contours even in completely homogeneous areas; in the center figure, a large rectangle is perceived, and, in the figure on the right, a white square partially occluded by a gray disk is perceived. These contours, which are defined without image gradient, are called "apparent" or "subjective" contours. Following convention, we distinguish, perhaps arbitrarily, between "modal completion", in which the goal is to construct a perceived boundary, and (as in Figure 1, left and center) and "amodal

completion", in which one reconstructs the shape of a partially occluded objects (as in Figure 1, right); see [1].

Our goal is to extract these internal objects, which is known as "segmentation." Since some information is missing, algorithms typically complete the segmentation process by building models of what happens between the available data. In this paper we propose a method for segmentation of images with missing boundaries. We take the following perspective:

- The observer is drawn to a reference point within the image; from that reference point the completion process is constructed.

- Thus, starting from this given reference point, we devise an algorithm which takes advantage of the available boundary data to construct a complete segmentation. Thus, in our approach, the computed segmentation is a function of the reference point.

We define a segmentation as a piecewise constant surface that varies rapidly across the boundary between different objects and stays flat within it. In [2] the segmentation is a piecewise smooth/constant approximation of the image. In our approach the segmentation is a piecewise constant approximation of the point of view- or reference surface. To obtain it we define the following steps:

1. Select a fixation point and build the point-of-view surface.

2. Detect local features in the image.

3. Evolve the point of view surface with a flow that depends both on the geometry of the surface and on the image features. The flow evolves the initial condition towards a piecewise constant surface.

4. (Automatically) Pick the level set that describes the desired object.

During the evolution, the point-of-view surface is attracted by the existing boundaries and steepens. The surface evolves towards the piecewise constant solution by continuation and closing of the boundary fragments and the filling in the homogeneous regions. A solid object is delineated

as a constant surface bounded by existing and recovered shape boundaries. With this method, the image completion process depends both on the point of view and on the geometric properties of the image. This observation is supported by experimental results on perceptual organization of the human visual system, as pointed out by Kanizsa: "if you fix your gaze on an apparent contour, it disappears, yet if you direct your gaze to the entire figure, the contours appear to be real,"[1].

Both the mathematical and algorithmic approach in our method relies on a considerable body of recent work based on a partial differential equations approach to both front propagation and to image segmentation. Level set methods, introduced by Osher and Sethian [3], track the evolution of curves and surfaces, using the theory of curve and surface evolution and the link between between front propagation and hyperbolic conservation laws discussed in [4, 5]. These methods embed the desired interface as the zero level set desired interface as the zero level set of an implicit function, and then employ finite differences to approximate the solution of the resulting initial value partial differential equation. Malladi, Sethian and Vemuri [6] and Caselles, Catte, Coll, and Dibos in [7] used this technology to segment images by growing trial shapes inside a region with a propagation velocity which depends on the image gradient and hence stops when the boundary is reached; thus, image segmentation is transformed into an initial value partial differential equation in which a propagating front stops at the desired edge.

In [8], Sochen, Kimmel, and Malladi view image processing as the evolution of an image manifold embedded in a higher dimensional Riemannian space towards a minimal surface. This framework has been applied to processing both single- and vector-valued images defined in two and higher dimensions (see [9]). We follow some of these ideas in this paper and view segmentation as the evolution of an initial reference manifold under the influence of local image features.

Our approach takes a more general view of the segmentation problem. Rather than follow a particular front or level curve which one attempts to steer to the desired edge (as in [10, 7]), we begin with an initial surface, chosen on the basis of a user-supplied reference fixation point. We then flow this *entire surface* under speed law dependent on the image gradient, without regard to any particular level set. Suitably chosen, this flow sharpens the surface around the edges and connects segmented boundaries across the missing information. On the basis of this surface sharpening, we can identify a level set corresponding to an appropriate segmented edge. We test our algorithm on

various figures, including those above, as well as medical images in which the signal to noise ratio is truly small and the most part of the edge is missed, as in the case of ultrasound images.

The paper is organized as the following. In Section 2 we review past work in segmentation of images with missing boundaries. In Section 3 we discuss the mathematical problem and we present a numerical method to solve it. In Section 4, results of the application of the method to different images and we discuss both the modal and amodal completion scenarios.

2 Past Work and Background

In this section, we review some of the other work that has attempted to recover subjective contours. In Mumford [11], the idea was that distribution of subjective contours can be modeled and computed by particles traveling at constant speeds but moving in directions given by Brownian motion. More recently, Williams and Jacobs [12, 13] introduced the notion of a stochastic completion field, the distribution of particle trajectories joining pairs of position and direction constraints, and showed how it could be computed. However, the difficulty with this approach is to consistently choose the main direction of particle motion; in other words, do the particles move parallel (as needed to complete Fig. 1, left) or perpendicular (as needed to complete 1, center) to the existing boundaries, i.e. edges? In addition, in this approach, what is being computed is a distribution of particles and not an explicit contour/surface, closed or otherwise. In this paper, we are interested in recovering explicit shape representations that are reproduce that of the human visual perception, especially in regions with no image-based constraints such as gradient jump or variation in texture.

A combinatorial approach is considered in [14]. A sparse graph is constructed whose nodes are salient visual events such as contrast edges and L-type and T-type junctions of contrast edges, and whose arcs are coincidence and geometric configurational relations among node elements. An interpretation of the scene consists of choices among a small set of labels for graph elements. Any given labeling induces an energy, or cost, associated with physical consistency and figural interpretation. This explanation follows the classical 2 1/2 D sketch of David Marr [15].

A common feature of both completion fields, combinatorial methods, as well as variational segmentation methods [2] is to postulate that the segmentation process is independent of observer's point of focus. On the other hand, methods based on active contours perform a segmentation

strongly dependent on the user/observer interaction. Since their introduction in [16], deformable models have been extensively used to integrate boundaries and extract features from images. An implicit shape modeling approach with topological adaptability and significant computational advantages has been introduced in [6, 7, 10]. They use the level set approach [3, 17] to frame curve motion with a curvature dependent speed. These and a host of other related works rely on edge information to construct a shape representation of an object. In the presence of large gaps and missing edge data, the models tend to go astray and away from the required shape boundary. This behavior is due to a constant speed component in the governing equation that helps the curve from getting trapped by isolated spurious edges. On the other hand, if the constant inflation term is switched off, as in [18, 19], the curve has to be initialized close to the final shape for reasonable results. Recently in [20] the authors use geometric curve evolution for segmenting shapes without gradient by imposing a homogeneity constraint, but the method is not suitable for detecting the missing contours shown in Figure 1.

The approach in this paper relies on the perspective that segmentation, regardless of dimensionality, is a 'view-point' dependent computation. The 'view-point' or the user-defined initial guess to the segmentation algorithm enters our algorithm via the point-of-view surface. Next, we evolve this reference surface according to a feature-indicator function. The shape completion aspect of our work is relies on two components: (1) the evolution of a higher-dimensional function and (2) a flow that combines the effects of level set curve evolution with that of surface evolution. In what follows, we will present a geometric framework that will make this possible. Computing the final segmentation (a contour or surface) is accomplished by merely plotting a particular level set of a higher dimensional function.

3 Theory

3.1 Local feature detection

Consider an image $\mathcal{I} : (x, y) \rightarrow I(x, y)$ defined in $M \subset R^2$. One initial task in image understanding is to build a representation of the changes and local structure of the image. This often involves detection of intensity changes, orientation of structures, T-junctions and texture. The result of this stage is a representation called *the raw primal sketch* [15]. Several methods have been proposed to

compute the raw primal sketch, including multiscale/multiorientation image decomposition with Gabor filtering [21], wavelet transform [22], deformable filter banks [23] etc. For the purpose of the present paper we consider a simple edge indicator, namely

$$g(x,y) = \frac{1}{1 + (|\nabla G_\sigma(x,y) \star I(x,y)|/\beta)^2}$$
$$G_\sigma(\xi) = \frac{\exp(-(\xi/\sigma)^2)}{\sigma\sqrt{\pi}} \tag{1}$$

The edge indicator function $g(x,y)$ is a non-increasing function of $|\nabla G_\sigma(x,y) \star I(x,y)|$, where $G_\sigma(x,y)$ is a gaussian kernel and $(\star)$ denotes the convolution. The denominator is the gradient magnitude of a smoothed version of the initial image. Thus, the value of g is closer to 1 in flat areas $(|\nabla I| \to 0)$ and closer to 0 in areas with large changes in image intensity, i.e. the local edge features. The minimal size of the details that are detected is related to the size of the kernel, which acts like a scale parameter. By viewing g as a potential function, we note that its minima denotes the position of edges. Also, the gradient of this potential function is a force field that always points in the local edge direction; see Figure 2.

To compute $\nabla G_\sigma(x,y) \star I(x,y)$, we use the convolution derivative property $\nabla G_\sigma(x,y) \star I(x,y) = \nabla(G_\sigma(x,y) \star I(x,y))$ and perform the convolution by solving the linear heat equation

$$\frac{\partial \varphi}{\partial t} = \nabla.(\nabla \varphi) \tag{2}$$

in the time interval $[0, \sigma]$ with the initial condition $\varphi(x,y,0) = I(x,y)$.

We conclude this subsection by observing that there are other ways of smoothing an image as well as computing an edge indicator function or in general a feature indicator function, see [18, 10, 24, 25, 26, 8, 9].

3.2 Global boundary integration

Now, consider a surface $S : (x,y) \longrightarrow (x,y,\Phi)$ defined in the same domain M of the image I. The differential area of the graph S in the Euclidean space is given by:

$$dA_E = \sqrt{1 + \Phi_x^2 + \Phi_y^2} \, dx \, dy \tag{3}$$

We will use the edge indicator g to stretch and shrink a metric appropriately chosen so that the edges act as attractors under a particular flow. With the metric g applied to the space, we have

$$dA_g = g(x, y)\sqrt{1 + \Phi_x^2 + \Phi_y^2} \; dx \; dy. \tag{4}$$

Now, consider the area of the surface

$$A_g = \int_M g(x, y)\sqrt{1 + \Phi_x^2 + \Phi_y^2} \; dx \; dy, \tag{5}$$

and evolve the surface in order to (locally) minimize it. The steepest descent of Eqn. 5 is obtained with usual multivariate calculus techniques and results in the following flow

$$\frac{\partial \Phi}{\partial t} = g\frac{(1 + \Phi_x^2)\Phi_{yy} - 2\Phi_x\Phi_y\Phi_{xy} + (1 + \Phi_y^2)\Phi_{xx}}{1 + \Phi_x^2 + \Phi_y^2} + (g_x\Phi_x + g_y\Phi_y)[1] \tag{6}$$

The first term on the right hand side is a parabolic term that evolves the surface in the normal direction under its mean curvature weighted by the edge indicator g. The surface motion is slowed down in the vicinity of edges ($g \to 0$). The second term on the right corresponds to pure passive advection of the surface along the underlying velocity field $-\nabla g$ whose direction and strength depend on position. This term pushes/attracts the surface in the direction of the image edges. Note that $g(I(x, y))$ is not a function of the third coordinate, therefore the vector field $-\nabla g$ lies entirely on the (x, y) plane.

The following characterizes the behavior of the flow (Eqn. 6):

1. In regions of the image where edge information exists, the advection term drives the surface towards the edges. The level sets of the surface also get attracted to the edge and accumulate. Consequently, the spatial gradient increases and the surface begins to develop a discontinuity. Now, when spatial derivatives $\Phi_x, \Phi_y \gg 1$, the Eqn. 6 approximates to

$$\frac{\partial \Phi}{\partial t} \approx g\frac{\Phi_x^2\Phi_{yy} - 2\Phi_x\Phi_y\Phi_{xy} + \Phi_y^2\Phi_{xx}}{\Phi_x^2 + \Phi_y^2} + (g_x\Phi_x + g_y\Phi_y). \tag{7}$$

which is nothing but the level set flow for shape recovery [27, 18]. In addition, the (parabolic) first term in Eqn. 7 is a directional diffusion term in the tangent direction and limits diffusion across the edge itself.

---

[1]Note that this is the mean curvature flow in a Riemannian space with conformal metric $g\delta_{ij}$.

2. The region inside the objects where $g \to 1, |\nabla g| \to 0$ the surface is driven by the Euclidean mean curvature motion towards a flat surface. In these regions we observe $\Phi_x, \Phi_y \ll 1$ and equation 6 approximates to:

$$\frac{\partial \Phi}{\partial t} \approx g(\Phi_{xx} + \Phi_{yy}) + (g_x \Phi_x + g_y \Phi_y). \tag{8}$$

The above equation is non-uniform diffusion equation and denotes the steepest descent of the weighted $L2$ norm, namely

$$\int g |\nabla \Phi|^2 \, dxdy. \tag{9}$$

If image gradient inside the object is actually equal to zero, then $g = 1$ and Eqn. 8) becomes a simple linear heat equation and the flow corresponds to linear uniform diffusion.

3. We now address the regions in the image corresponding to subjective contours. In our view, subjective contours are simply continuation of existing edge fragments. As we explained before, in regions with well defined edge information, Eqn. 6 causes the level curve accumulation thereby causing an increase in the spatial gradient of Φ. Due to continuity in the surface, this edge fragment information is propagated to complete the missing boundary. The main equation 6 is a mixture of two different dynamics, the level set flow (7) and pure diffusion (8) and locally, points on the Φ surface move according to one of these mechanisms. In steady state solution, the points inside the objects are characterized by pure linear diffusion, while points on the boundary are characterized by the level set edge enhancing flow. The scaling of the function Φ wheights the two dynamics. If Φ is "narrow range" (contains a narrow range of values) then the derivatives are small and the behaviour of the flow (6) is mostly diffusive. In the opposite when Φ is "wide range" the behaviour is mostly like level set plane curve evolution. We perform the scaling by multiplying the initial surface (x, y, Φ_0) (point of view surface) with a scaling factor α.

3.3 Numerical Scheme

In this subsection, we show how to approximate equation (6) with finite differences. Let us consider a rectangular uniform grid in space-time (t, x, y); then the grid consists of the points $(t_n, x_i, y_j) =$

8

$(n\Delta t, i\Delta x, j\Delta y)$. We denote with Φ_{ij}^n the value of the function Φ at the grid point (t_n, x_i, y_j). The first term of (6) is a parabolic contribution to the equation of motion and we approximate this term with central differences. The second term on the right corresponds to passive advection along an underlying velocity field ∇g whose direction and strength depend on edge position. This term can be approximated using the upwind schemes; here we borrow the techniques described in [17, 3]. In other words, we check the sign of each component of ∇g and construct one-sided difference approximation to the gradient in the appropriate (upwind) direction. With this, we can write the complete first order scheme to approximate equation (6) as follows:

$$\Phi_{ij}^{n+1} = \Phi_{ij}^n + \Delta t \left\{ \begin{bmatrix} g_{ij} \frac{(1+D_{ij}^{0x^2})D_{ij}^{0yy} - 2D_{ij}^{0x}D_{ij}^{0y}D_{ij}^{0xy} + (1+D_{ij}^{0y^2})D_{ij}^{0xx}}{1+D_{ij}^{0x^2}+D_{ij}^{0y^2}} \end{bmatrix} \\ - \begin{bmatrix} [max(g_{ij}^{0x}, 0)D_{ij}^{-x} + min(g_{ij}^{0x}, 0)D_{ij}^{+x} \\ +max(g_{ij}^{0y}, 0)D_{ij}^{-y} + min(g_{ij}^{0y}, 0)D_{ij}^{+y}] \end{bmatrix} \right\} \tag{10}$$

where D is a finite difference operator on Φ_{ij}^n, the superscripts $\{-, 0, +\}$ indicate backward, central and forward differences respectively, and the superscripts $\{x, y\}$ indicate the direction of differentiation. We impose Dirichlet boundary conditions by fixing the value on the boundary equal to the minimum value of the point-of-view surface.

4 Results

In this section, we present results of several computations aimed at performing both modal and amodal completion of objects with missing boundaries. The approach consists of a user-defined point-of-view or a reference surface and an edge indicator function computed as a function of the image. Different choices exist for the reference surface; we show two of them in Fig. 3. In the next examples we use $\Phi_0 = \alpha/\mathcal{D}$, where $\mathcal{D}$ is the distance from the initial point of view and α is a scaling factor; $\alpha = 10^3$ is the fixed value that we use. First, we consider the classical triangle of Kanizsa (Fig. 1) and apply the algorithm in order to perform a modal completion of the missing boundaries. We compute the edge map as shown in the left image of Fig. 4 and then choose a reference point approximately at the center of the perceived triangle (center image of Fig. 4). The evolution of the surface under the flow induced by Eqn. 6 is visualized in Fig. 5. The so called subjective surface is the steady state piece-wise linear surface shown at the end of this sequence. The triangle boundary shown in the right image of Fig. 4 is found by plotting the level set $\bar{\Phi} = \{max(\Phi) - \epsilon\}$

of the subjective surface. Note that in visualizing the surface, we normalize it with respect to its maximum.

Next, we present a series of results of computing subjective surfaces. In Fig. 6, we show the subjective surface computation from an image with little or no (aligned) edge information. We render the perceived square in the final image of Fig. 6.

The subjective contours we have considered so far are called "modal" contours because they are "perceived" in the visual experience. Now we consider "amodal" contours that are present in images with partially occluded shapes. Consider the example of a white square partially occluded by a gray disk as shown in Fig. 7. Our goal is to recover the shapes of both the square and the disk. We employ a three step procedure: first, we build the edge map g_1 of the image and choose a point of focus inside the disk and perform the segmentation of the grey disk O_{disk}. Second, we build another edge map $g_2 = \begin{cases} 1 & (x, y) \in O_{disk} \\ g_1 & otherwise \end{cases}$ so that all the image features belonging to the first object are inhibited in the new function. As the third step we perform the modal completion of the partially occluded square using the new edge map g_2. Again, the process is completely automatic after the initial point of reference and the entire process is shown in Fig. 7.

Echographic images are difficult candidates for shape recovery because they possess highly noisy structures and large parts of the boundary are often found absent thereby making shape recovery very difficult. We are interested in developing segmentation methods that deal with non-continuous edges in extremely noisy images. In Fig. 8, we show one such computation; we use a line initialization instead of a fixation point and the point-of-view surface is constructed to be the distance function from this initial line. The final result, a particular level set of the the subjective surface is shown in the right image of Fig. 8.

5   Acknowledgements

References

[1] Kanizsa,G. (1976) Scientific American, pp. 48-52.

[2] Mumford,D., Shah,J. (1989) Communications on Pure and Applied Mathematics, Vol. XLII, pp. 577-685.

[3] Osher,S., Sethian,J.A. (1988) Journal of Computational Physics, Vol. 79, pp.12-49.

[4] Sethian, J.A. (1985) Comm. Math. Phys., Vol.101, pp. 487-499.

[5] Sethian, J.A. (1987) in Variational Methods for Free Surface Interfaces, Eds. P. Concus and R. Finn, (Springer-Verlag, NY).

[6] Malladi,R., Sethian,J.A., Vemuri,B. (1993) SPIE Proceedings on Geometric Methods in Computer Vision II, San Diego, pp. 246-258.

[7] Caselles,V., Catte',F., Coll,T., Dibos,F. (1993) Numerische Mathematik,Vol.66, pp.1-31.

[8] Sochen,N., Kimmel,R., Malladi,R. (1998) IEEE Transactions on Image Processing, Vol. 7, N. 3, pp.310-318.

[9] Kimmel,R., Malladi,R., Sochen, N. (2000) to appear in *International Journal of Computer Vision,*

[10] Malladi,R., Sethian,J.A., Vemuri,B.C. (1995) IEEE Transactions on Pattern Analysis and Machine Intelligence, Vol.17, N.2.

[11] Mumford,D. (1994) Algebraic Geometry and Its Applications, Chandrajit Bajaj (ed.), (Springer-Verlag, New York).

[12] Williams,L.R., Jacobs,D.W. (1997) Neural Computation, Vol.9, N.4,pp.837-858.

[13] Williams,L.R., Jacobs,D.W. (1997) Neural Computation, Vol.9, N.4,pp.859-881.

[14] Saund, E. (1999) CVPR.

[15] Marr,D. (1982) *Vision*, (W.H. Freeman & Co., San Francisco).

[16] Kass,M., Witkin,A., Terzopoulos,D. (1988) IJCV, Vol.1,N. 4,pp.321-331.

[17] Sethian,J.A. (1999) *Level Set Methods and Fast Marching Methods*, (Cambridge University Press).

[18] Caselles,V., Kimmel,R., Sapiro,G. (1997) IJCV, Vol.22,N.1,pag.61-79.

[19] Sarti,A., Malladi,R., (2000) LBNL-44442, Lawrence Berkeley National Laboratory, October 1999; to appear in *Geometric Methods in Bio-Medical Image Processing*, Ed. R. Malladi, Springer Verlag.

[20] Chan,T.F, Vese,L.A. (1998) CAM Report 98-53, UCLA Dept. of Mathematics.

[21] Gabor,D. (1946) *Theory of communication*, J. Inst. Elect. Eng., Vol. 93, pp. 429-457.

[22] Lee,T.S. (1996) IEEE Transaction on Pattern Analysis and Machine Intelligence, Vol.18, N.10, pp. 959-971.

[23] Perona,P., (1995) IEEE Transactions on Pattern Analysis and Machine Intelligence, Vol.17, N.5, pp. 488-499.

[24] Malladi,R., Sethian,J.A. (1996) Graphical Models and Image Processing, Vol. 38(2) pp. 127-141.

[25] Perona,P., Malik,J. (1987)

   In Proc. IEEE Computer Society Workshop on Computer Vision.

[26] Sarti,A., Mikula,K., Sgallari,F. (1999) IEEE Transactions on Medical Imaging, Vol. 18, n. 6, pag. 453-466.

[27] Malladi,R., Sethian,J.A., (1998) in *Proceedings of ICCV'98*, pp. 304–310, Mumbai, India.

Figure Captions

Figure 1. Three images with subjective contours.

Figure 2. Local edge detection: The edge map g and its spatial gradient $-\nabla g$.

Figure 3. Point-of-view surfaces: on the left $\Phi_0 = -\alpha \mathcal{D}$, where $\mathcal{D}$ is the distance function from the fixation point, and on the right $\Phi_0 = \alpha/\mathcal{D}$.

Figure 4. Three steps of the modal completion of the triangle of Kanizsa: on the left the edge indicator $-\nabla g(I)$ is shown, in the center a set of equispaced contour lines of the point-of-view surface are drawn, and on the right is the level set of the subjective surface that corresponds to the triangle boundary.

Figure 5. Four time frames showing the evolution of the point-of-view surface (upper left) towards the subjective surface (bottom right). In this visualization the original image has been texture mapped onto the surface.

Figure 6. Modal completion of an image without any aligned gradient.

Figure 7. Amodal completion of the white square partially occluded by the gray disk. In the first row the original image (left) and the point-of-view surface (center, right) are shown. In the second row, the edge map g_1 (left), the subjective surface (center), and the occluding disk boundary (right) are shown. The amodal completion of the square is shown in the third row. The new edge map g_2 (left) is obtained from the previous one by simply removing the features corresponding to the occluding object (disk). This new edge map allows the formation of a new subjective contour (center) and the square boundary (right). We use the value $\beta = 0.3$ in the edge indicator.

Figure 8. Segmentation of fetal echogram: modal completion is needed to recover a large portion of the missing boundary in the dorsal section of the fetus. The original image (left), the line of view (center) and the segmented boundary (right) are shown.

Figure 1: Three images with subjective contours.

Figure 2: Local edge detection: The edge map g and its spatial gradient $-\nabla g$.

Figure 3: Point-of-view surfaces: on the left $\Phi_0 = -\alpha\mathcal{D}$, where $\mathcal{D}$ is the distance function from the fixation point, and on the right $\Phi_0 = \alpha/\mathcal{D}$.

Figure 4: Three steps of the modal completion of the triangle of Kanizsa: on the left the edge indicator $-\nabla g(I)$ is shown, in the center a set of equispaced contour lines of the point-of-view surface are drawn, and on the right is the level set of the subjective surface that corresponds to the triangle boundary.
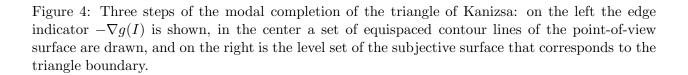
Figure 5: Four time frames showing the evolution of the point-of-view surface (upper left) towards the subjective surface (bottom right). In this visualization the original image has been texture mapped onto the surface.

Figure 6: Modal completion of an image without any aligned gradient.

Figure 7: Amodal completion of the white square partially occluded by the gray disk. In the first row the original image (left) and the point-of-view surface (center, right) are shown. In the second row, the edge map g_1 (left), the subjective surface (center), and the occluding disk boundary (right) are shown. The amodal completion of the square is shown in the third row. The new edge map g_2 (left) is obtained from the previous one by simply removing the features corresponding to the occluding object (disk). This new edge map allows the formation of a new subjective contour (center) and the square boundary (right). We use the value $\beta = 0.3$ in the edge indicator.

Figure 8: Segmentation of fetal echogram: modal completion is needed to recover a large portion of the missing boundary in the dorsal section of the fetus. The original image (left), the line of view (center) and the segmented boundary (right) are shown.